

Raman microspectroscopy of diamond crystals and thin films prepared by hot-filament-assisted chemical vapor deposition

A. M. Bonnot*

Laboratoire d'Etudes des Matériaux Minces, Centre d'Etudes Nucléaires de Grenoble du Commissariat à l'Energie Atomique (CEA/DMG), Boîte Postale 85X, 38041 Grenoble CEDEX, France

(Received 21 April 1989; revised manuscript received 10 October 1989)

Diamond crystals and thin films were prepared by thermal decomposition of methane and hydrogen, in the presence of a hot tungsten filament. Raman microspectroscopy investigations were carried out and correlated to scanning-electron-microscopy observations of the crystallization. It is shown that the diamond Raman signal of individual cubo-octahedric crystals depends on their orientation with respect to the substrate and on disorder upon growth. The influence of growth processes on the diamond Raman signal is considered and, in particular, contamination effects by hydrogen and tungsten impurities are emphasized. As the film crystallization deteriorates from an assembly of faceted crystals to that of blunted crystals and then to that of ball-like elements, the intensity of the diamond Raman line decreases and broad bands appear. The appearance of these broad bands is attributed to the presence of an amorphous carbon phase with atoms hybridizing with sp^2 and sp^3 bonds.

INTRODUCTION

Under normal thermodynamic conditions, graphite is the stable phase of solid carbon. Diamond is the high-temperature and high-pressure (HT,HP) thermodynamical phase. Diamond exists in two crystallographic forms: cubic and hexagonal. The cubic diamond form is the most commonly encountered. In nature it has a volcanic origin, while the hexagonal form (lonsdaleite) has been found only in meteorites. Usually, the term "diamond" is set for the cubic form, to which we will be referring. The crystallographic form will be explicated only for the hexagonal phase.

The interest in diamond synthesis is due to its excellent extrinsic physical and chemical properties. Essentially because of the very strong covalent bond between the carbon atoms, diamond shows exceptional insulating properties. It is the hardest known material. It combines optical transparency from ultraviolet (the optical gap is 5.5 eV) to infrared, high electron and hole mobilities, and very good thermal conductivity. It is also chemically inert. When doped with boron, it becomes semiconducting with a shallow donor level (0.4 eV). For all these reasons, the technical challenge of diamond synthesis, in the form of films, is very attractive. Diamond thin-film technology is of particular interest in the field of optical components for aerospace applications and can also play a very important role in the field of electronics.

The first successes in diamond synthesis at low temperature and low pressure, in the metastable phase, were reported in the Soviet Union by Deryagin¹ in 1956 and in the United States by Eversole² in 1958. Diamond growth on diamond seeds was obtained from a mixture of hydrocarbon and hydrogen, below or close to the atmospheric pressure at about 1000 °C. Since then, diamond-film synthesis at low pressure and low temperature has been at-

tempted by using various preparation techniques. Among the techniques employed, it seems that only chemical vapor deposition (CVD) can lead to the synthesis of pure diamond films, whether they are hot-filament assisted,³⁻⁸ microwave-plasma assisted,⁹⁻¹⁶ plasma-laser assisted,¹⁷ or dc-plasma assisted.¹⁸ Whatever the CVD technique used, diamond synthesis requires certain experimental conditions: a mixture of hydrocarbon and hydrogen with a very low proportion of hydrocarbon ($\leq 1\%$) and a substrate temperature of about 600-1000 °C.

Alternatives to CVD techniques, which require a high substrate temperature, are the C^+ (Refs 19 and 20) or C^- (Ref. 21) preparation methods at room temperature. Other techniques, such as dc or rf sputtering or CVD with a low substrate temperature, generally lead to a carbon solid phase $a-C:H$.²² When the deposition is made in the presence of ions, $i-C$ films (for ion) are obtained.²³ The structure of this type of film is not yet well understood. However, they are often nonhomogeneous and may contain diamond particles. More generally, films which have physical and chemical properties more or less close to that of diamond are named diamondlike carbon (DLC).²⁴

The different states of crystallization encountered in DLC films are the consequence of allotropic forms of solid carbon: diamond, graphite, and carbene, which can be defined by the types of bonds between carbon atoms. In diamond, each of the four valence electrons is in an sp^3 configuration and is engaged in a σ covalent bond with a neighboring atom. This corresponds to a tetrahedral configuration of the carbon atoms. In graphite, three of the valence electrons are engaged in σ bonds with neighboring atoms. In the basal plane, the carbon atoms are in an sp^2 tetragonal configuration. The fourth electron is in a π orbital, perpendicular to the basal

planes which are weakly bonded with each other. Carbine denomination embraces all different valence-electron hybridizations: sp^2 , and sp^3 .

Because of all the hybridizations encountered which confer different physical and chemical properties on solid carbon phases, it is interesting to look at the nature of the bonding in the film. This can be done with experiments whose signal depends on the density of valence states and/or conduction states, such as ultraviolet photoemission (UPS), inverse UPS, and electron-energy-loss spectroscopy (EELS). Raman spectroscopy is also a very well-suited experimental technique. The Raman signal corresponds to inelastically scattered light resulting from the radiative emission of dipoles induced by the electric field of the incident light and coupled with atomic vibrations. With Raman spectroscopy, diamond, which has a phonon density of states very different from other carbon phases, can be detected without any ambiguity. The Raman signal is very sensitive to short-range disorder and consequently, it can reveal different forms of amorphous carbon: a -C or a -C:H. One of the advantages of Raman spectroscopy is that it does not require special preliminary film treatment, the experiment being insensitive to surface effects.

In a previous paper,²⁵ results on diamond synthesis with a hot-filament-assisted CVD technique were presented. The influence of experimental conditions on scanning-electron-microscopy (SEM) morphology and on the Raman spectra were analyzed. The results of SEM and Raman spectroscopy were correlated. However, these two characterizations were not performed on the same scale: the argon laser light of the Raman apparatus was focused on an area of $\sim 100 \mu\text{m}^2$, whereas SEM showed more or less faceted elements with dimensions of only a few micrometers.

In order to go further in our interpretation, Raman microspectroscopy investigations have been carried out. As will be shown, this method is appropriate because of the spatial resolution, which is of the same order as the dimension of the deposited elements in the films. In Sec. I, the preparation technique and the Raman microspectrophotometer are briefly described. In Sec. II, experimental conditions for diamond growth are presented. In Sec. III, Raman microspectra of deposited crystals of a few micrometers in size and in different shapes are described. The influence of bonding (graphitelike or diamondlike) on the Raman spectra and its modification by defect inclusions, hydrogenation, and amorphization are analyzed.

II. EXPERIMENT

A. Preparation technique

Diamond films were deposited by hot-filament-assisted CVD. The tungsten filament was placed 1 cm in front of the substrate. Methane and hydrogen were introduced near and between the filament and the substrate. The total pressure was 3000 Pa and the total flow rate was 15 sccm (cubic centimeters per minute at STP). The proportion of methane in hydrogen was varied between 1 and 4

vol % Si(100) wafers, Mo foils, or Mo films deposited on stainless steel were used as substrates. Electron bombardment of the substrate was achieved by positively polarizing it to 200 V. During deposition, the substrate temperature was kept constant by control of the oven surrounding the whole system which was placed in a quartz tube. Most of the depositions were done with a 1100-K substrate temperature, a 2400-K filament temperature, and a 3-h reaction time. Prior to deposition, the whole system was evacuated to 10^{-4} Pa and heated up to 1270 K.

B. Raman spectrophotometer

Raman microspectroscopy has been carried out with a Dilor Laser Raman Modular XY spectrophotometer. The region of observation was located with a standard optical microscope, operating in reflection. The halogen light of the optical microscope was replaced by the argon laser light with exactly the same light path through the microscope and the laser light was focused exactly at the region of observation. Areas as small as $1 \mu\text{m}$ were probed. After reflection from the sample and passing through the microscope, the scattered light was analyzed with a double subtractive monochromator, used with a large band filter to eliminate the laser light. A multichannel detector, mounted with 512 elements, was directly interfaced with a computer which controlled the position of different optical elements and processed the data.

III. EXPERIMENTAL RESULTS

A. Conditions for diamond growth—SEM and RHEED results

As experimental conditions for diamond growth with the hot-filament-assisted CVD technique have already been described elsewhere,²⁵ only the most important experimental parameters are presented here. Diamond growth depends crucially on the filament-to-substrate distance, the filament temperature, and the methane proportion in hydrogen. With a 1 vol % methane concentration in hydrogen, diamond growth was obtained with the filament heated up to 2400 K. The substrate temperature was in the range of 1000–1200 K. Bombardment of the positively polarized substrate by electrons increased the diamond nucleation rate.²⁶ However, without scratching the substrate, the nucleation rate remained low (Fig. 1). To obtain a continuous film (Fig. 2) the substrate had to be scratched with $1\text{-}\mu\text{m}$ diamond paste prior to the deposition.

Reflection-high-energy electron diffraction (RHEED) measurements made on all deposits indicated only diamond crystallization;²⁵ but SEM observations showed that the crystal morphology was inhomogeneous. SEM observation of a discontinuous deposit (see Fig. 1) showed isolated cubo-octahedric crystals with various orientation to the substrate. In Fig. 1(b), the crystal presents a (100) face parallel to the substrate; but in Fig. 1(c), it shows four tilted front faces: two(100) and two (111). Twinned (111) faces are also often observed. With the above experimental conditions used, films were inhomogeneous on an area of 1 cm^2 . The morphology varied continuously

from that of well-faceted crystals (Fig. 2) to that of blunted crystals (Fig. 3) and to that of ball-like elements (Fig. 4). The biggest crystals which are shown in Fig. 5 have been found on the edges of a Si(100) substrate. They are implanted into the substrate in such a way that only a half a cubo-octahedron is apparent.

B. Raman microspectroscopy

The laser light of the Raman apparatus has been focused onto a large number of individual crystals using the optical microscope. The Raman signal has been shown to be extremely sensitive to the crystal morphology and always differs in some ways from that of natural dia-

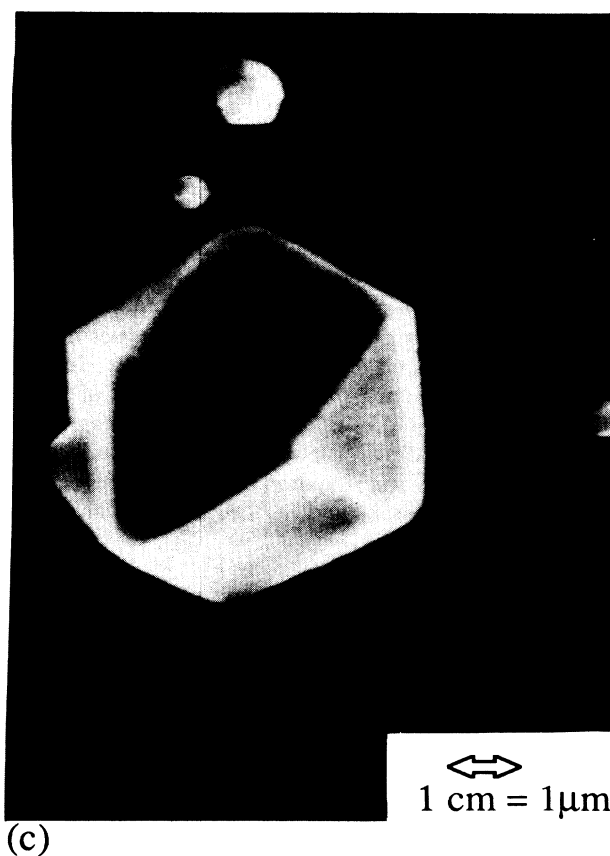
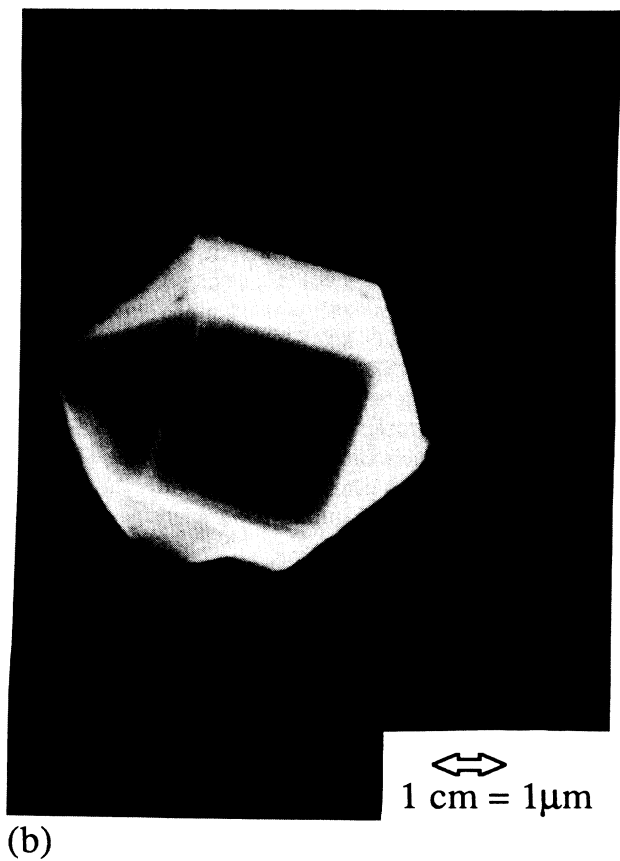
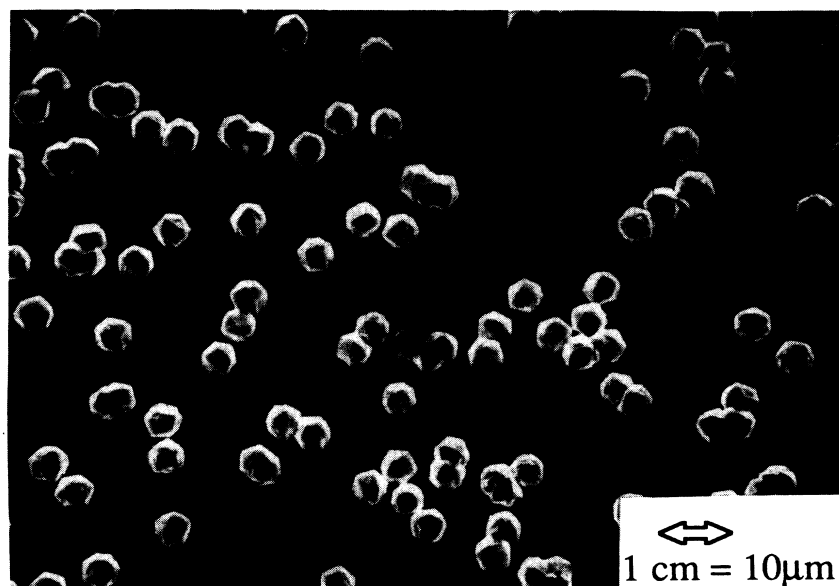


FIG. 1. SEM micrograph of diamond crystals on silicon.

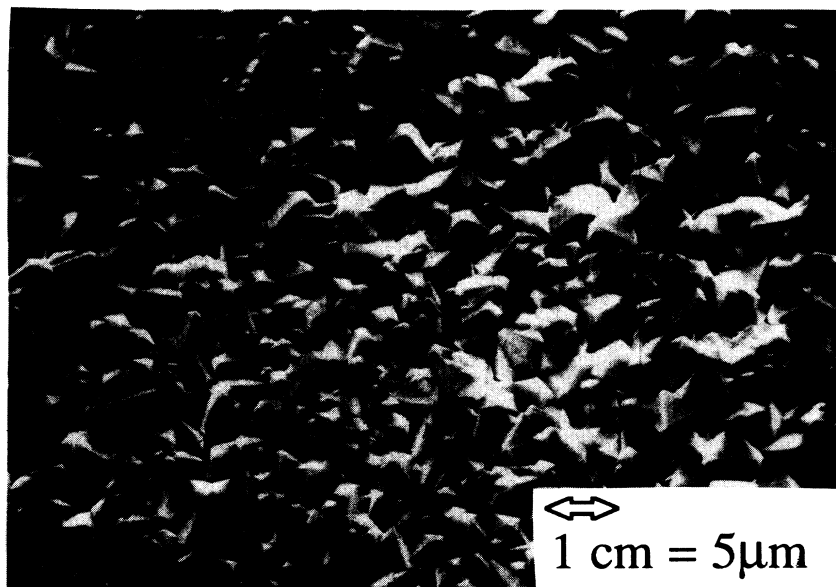


FIG. 2. SEM micrograph of a diamond thin film on a silicon substrate polished with $1\text{-}\mu\text{m}$ diamond paste.

mond. This manifests itself by variations of the Raman diamond-line position and width, and by the appearance of broad bands as the crystals lose their edges.

1. Raman spectra of cubo-octahedric crystals

The Raman spectra of cubo-octahedric CVD crystals which show, by means of the optical microscope of the Raman apparatus, well-defined crystallographic planes in front of the substrate, are represented in Fig. 6. Their characteristics are indicated in Table I and are compared to those of natural diamond, determined with the same experimental conditions.

The position of the diamond Raman line of CVD crystals varies from 1323 to 1336 cm^{-1} ; the narrowest line has a full width at half maximum (FWHM) of 8.5 cm^{-1} , the broadest has 21 cm^{-1} FWHM. These variations are well above the resolution of the Raman apparatus. As the width of the diamond line increases, two broad bands, at about 1540 and 1350 cm^{-1} grow up. Furthermore, the variation of the position and width of the diamond structure has been correlated to the crystal morphology.

Raman spectrum (a) in Fig. 6 corresponds to well-faceted cubo-octahedric crystals with a (100) front face parallel to the substrate. It is very similar to that of natural diamond, which indicates that only the diamond

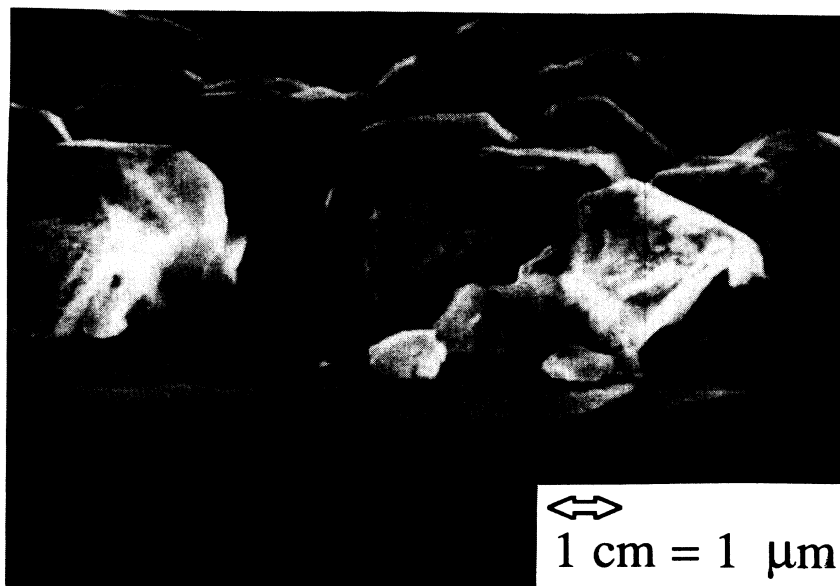


FIG. 3. SEM micrograph of diamond crystals which have lost their edges.

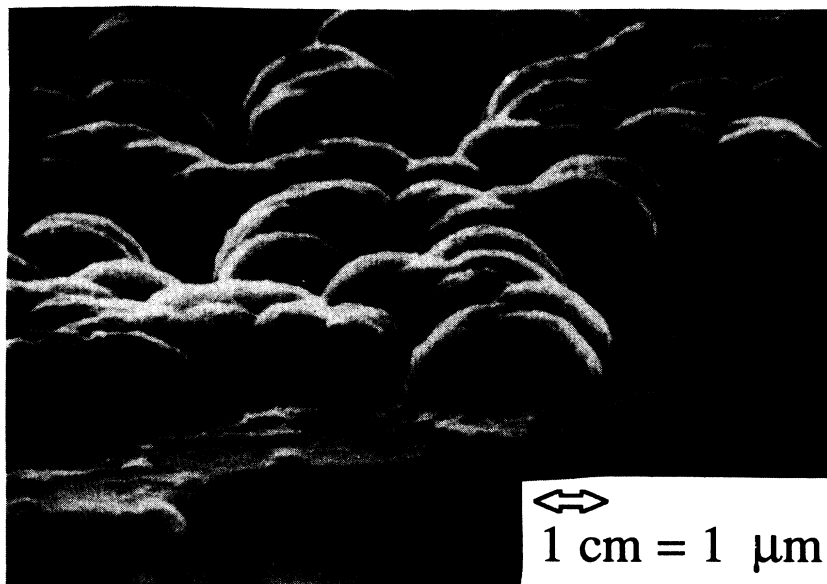


FIG. 4. SEM micrograph of carbon ball-shaped elements.

phase was formed. However, the Raman structure has a FWHM $\Delta\nu$ of at least 8.5 cm^{-1} [Table I, (a)] which is larger than that of natural diamond. The position ν^0 at maximum intensity is also slightly shifted to a lower wave number. Considering ν^+ and ν^- wave numbers at FWHM, it appears that broadening of the CVD diamond Raman line occurs essentially on the low-wave-number side [ν^+ value is the same as in natural diamond (1334 cm^{-1}), but a shift to lower ν^- values (1325.5 cm^{-1}) is evident when compared to natural diamond (1329 cm^{-1})].

Spectra (b)–(d) in Fig. 6 [their characteristics are indicated in Table I, (b)–(d)] also correspond to crystals with

a flat (100) front face parallel to the substrate, but with increasing disorder. It manifests itself by roughening of the crystal sides showing small grains with no well-defined crystallographic planes. With roughening of the crystal sides there is an increase of $\Delta\nu$ [Table I, (b)–(d)]. When compared to the Raman-spectrum characteristics of well-faceted crystals [Table I, (a)], one sees the following modifications of the diamond structure with crystal morphology: In spectrum (b), it is broadened (and slightly shifted) towards lower wave numbers; in spectrum (c), it is shifted towards lower wave numbers; in spectrum (d), it is broadened on both the high and low wave number sides.

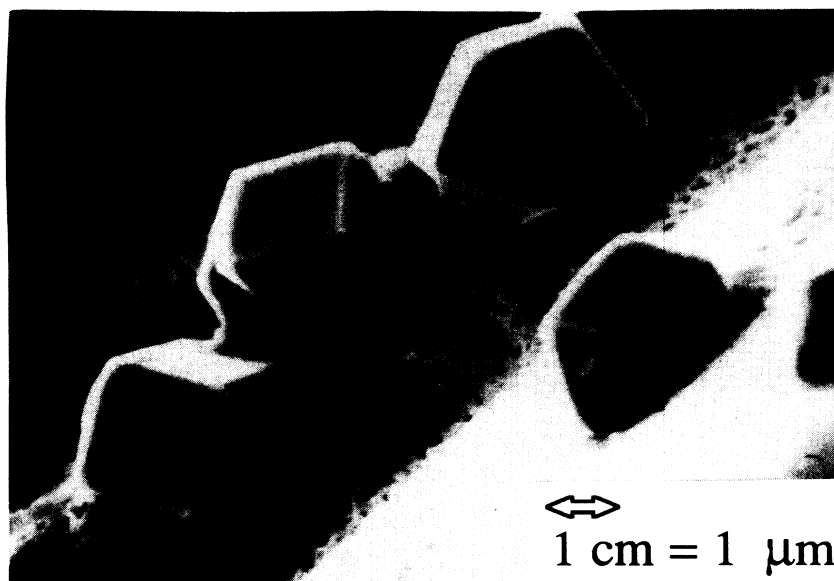


FIG. 5. SEM micrograph showing the way crystals are implanted in the edges of a silicon substrate.

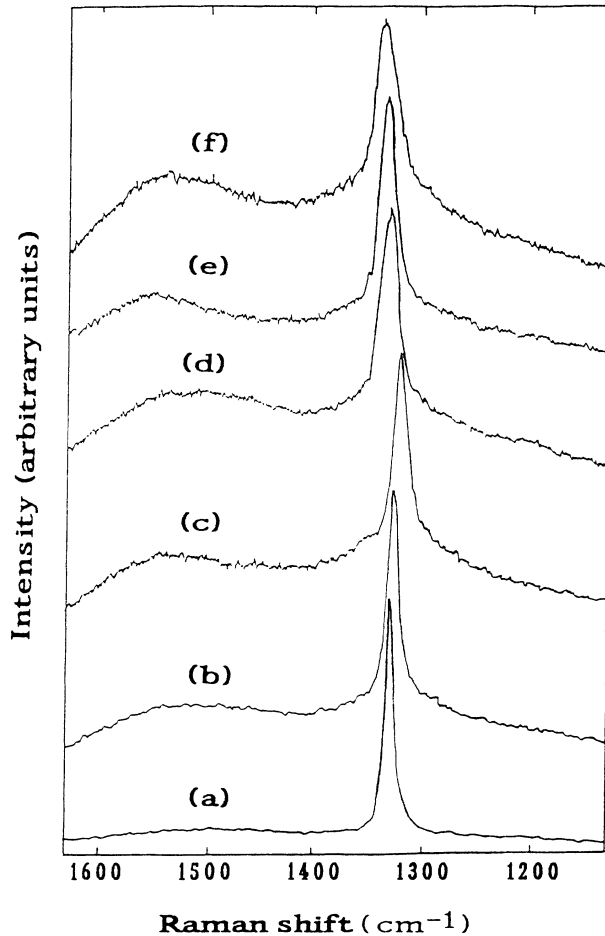


FIG. 6. Development of a Raman spectrum of diamond crystals with orientation to the substrate: (a)–(d), crystals with a (100) front face to the substrate but with increasing disorder upon growth from (a) to (d); (e), crystal with five twinned (111) front faces to the substrate; (f), crystal with 4 front faces to the substrate [two (111) and two (100)].

Raman spectrum (e) in Fig. 6 has been obtained for a crystal with five twinned (111) faces in front of the Si(100) substrate. From Table I (e) it is seen that the Raman diamond line has a maximum intensity at exactly the same ν^0 position as in natural diamond; but its width $\Delta\nu$ is

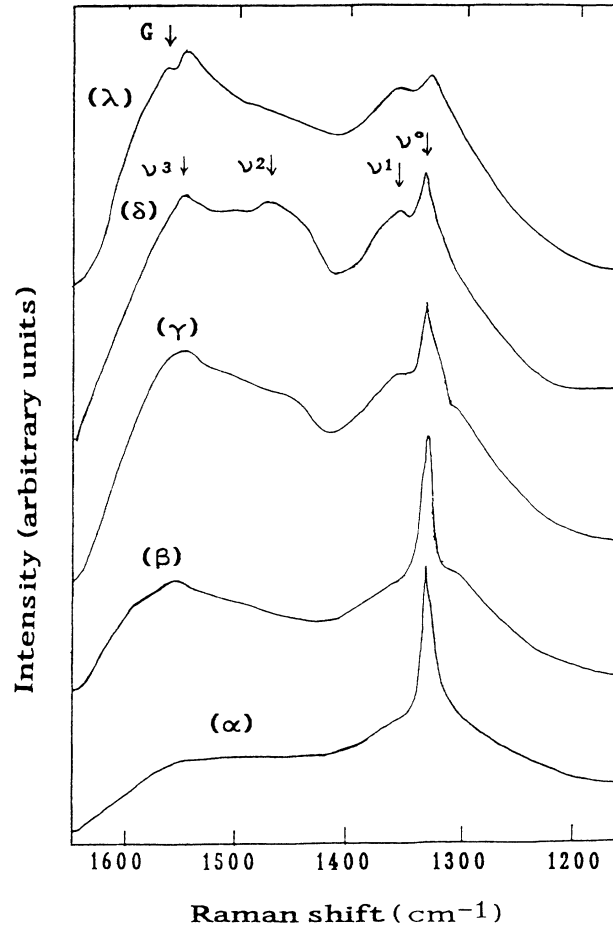


FIG. 7. Raman spectra of diamond thin films, prepared with a 1% vol methane concentration in hydrogen and formed with faceted crystals (α), blunted crystals (β) and (γ), and ball-shaped elements (δ). By comparison, the Raman spectrum (λ) of a deposit prepared with a 4 vol % methane concentration is also drawn.

larger, and broadening occurs on both the high and low wave number sides.

Spectrum (f) in Fig. 6 corresponds to cubo-octahedral crystals oriented to the substrate as in Fig. 1(c). Through the optical microscope of the Raman apparatus, four

TABLE I. Raman spectra of diamond crystals: (a)–(d), crystals with a (100) front face parallel to the substrate; (e), crystal with 5 twinned (111) front faces to the substrate; (f), crystal with four front faces to the substrate [two (111) and two (100)]. The diamond line has a maximum intensity located at ν^0 and a FWHM of $\Delta\nu = \nu^+ - \nu^-$.

	Substrate	ν^0 (cm ⁻¹)	$\Delta\nu$ (cm ⁻¹)	ν^+ (cm ⁻¹)	ν^- (cm ⁻¹)
Natural diamond		1332	5	1334	1329
(a)	MO	1330	8.5	1334	1325.5
(b)	Si	1328	12	1335	1323
(c)	Si	1323	13	1328	1315
(d)	Mo	1330	17	1340	1323
(e)	Si	1332	17	1340.5	1323.5
(f)	Si	1336	21.5	1345.5	1324

TABLE II. Raman-spectrum characteristics of films prepared with a 1 vol % methane concentration: (α), faceted crystals; (β) and (γ), blunted crystals; (δ), ball-shaped elements. The diamond Raman line has a maximum intensity $I(\nu^0)$ at ν^0 and a FWHM of $\Delta\nu$. The broad bands have a maximum intensity $I(\nu^i)$ at ν^i ($i=1,2,3$). By comparison, characteristics of the Raman spectrum (λ) of a carbon ball prepared with a 4 vol % methane concentration in hydrogen are also given. (G is the Raman band of graphite.)

	ν^0 (cm^{-1})	$\Delta\nu$ (cm^{-1})	ν^1 (cm^{-1})	ν^2 (cm^{-1})	ν^3 (cm^{-1})	G (cm^{-1})	$\frac{I(\nu^0)}{I(\nu^1)}$
(α)	1328	12	1500				2.3
(β)	1330	12	1540		1355		1.8
(γ)	1328	15	1540		1350		1.1
(δ)	1330		1540	1470	1355		1.0
(λ)	1324		1545	1470		1570	

front faces are observed: two (100) and two (111). The diamond Raman structure is now shifted to higher wave numbers and is broadened on the high-wave-number side [Table I (f)].

2. Raman-spectra modifications with crystallization state: From well-faceted crystals to blunted crystals and to carbon ball-like elements

Figure 7 shows Raman-spectrum development with crystal shape from faceted crystals (α) to blunted crystals (β), (γ), and to ball-like elements (δ). Spectral characteristics are indicated in Table II.

As crystals lose their edges [from (α) to (δ)], the intensity of the Raman diamond line decreases and broad bands appear. Faceted crystals with disorder upon growth or slightly blunted crystals give two broad Raman bands at about 1500–1540 and 1325–1355 cm^{-1} . As crystals become more blunted (γ) and even ball-like (δ), a third broad band appears at 1470 cm^{-1} , with an intensity that grows with deterioration in crystallization.

IV. DISCUSSION

The interaction of the electric field of the incident laser light of the Raman apparatus with electrons induces dipoles. In a solid, the Raman signal is the part of the dipole light emission which is inelastically scattered by the interaction with optical phonons. The Raman efficiency depends on the polarizability of the solid and on electron-phonon interaction. The Raman spectrum presents structures which are characteristic of the phonon density of states. In particular, results on Raman spectroscopy of the different allotropic forms of solid carbon, which have very different phonon density of states, are demonstrative.

A. Raman spectra of the allotropic forms of solid carbon

1. Raman spectrum of bulk diamond (synthetic and natural)

From the knowledge of the diamond (cubic) crystallographic structure and the symmetry rules of the Raman effect, it is clear that there is only one active phonon mode: $\Gamma_{25}'(F_{2g})$. This is a triply degenerate center-

phonon mode. The one-phonon Raman spectrum of diamond²⁷ is composed of a single structure at 1332.5 cm^{-1} , with a 1.65- cm^{-1} FWHM at room temperature.

The Raman spectrum of bulk diamond depends on temperature, applied pressure, and carbon isotope concentration.

(i) With temperature, the Raman shift decreases and the width of the Raman line increases.²⁷

(ii) Applying pressure or uniaxial compressive stress²⁸ splits the Γ_{25}' mode into a singlet LO mode and a doublet TO mode. Both modes are shifted to high energy by the hydrostatic component of the applied stress. In the back-scattering geometry, only the singlet mode is observed. Consequently, the Raman diamond shift increases (and the linewidth increases) with pressure.

(iii) Natural diamond is essentially formed with ^{12}C isotope and contains only 1.1% ^{13}C isotope. When doping synthetic diamond with ^{13}C , there is a monotonic decrease of the Raman shift and linewidth.²⁹ With a 15% ^{13}C concentration, the one-phonon line is at 1328 cm^{-1} . Increasing ^{13}C isotope concentration to 36% shifts the Raman line to 1318.6 cm^{-1} .

The Raman spectrum of hexagonal diamond powder formed under shock-induced high pressure³⁰ is composed of a broad band ($\Delta\nu \geq 30 \text{ cm}^{-1}$) whose position varies from particule to particule from 1315 to 1326 cm^{-1} . However, the ureilite meteorites which contain diamond with the presence of the hexagonal form³¹ give a Raman line very similar to that of CVD diamond: it is centered at 1330 cm^{-1} and has a $\sim 10\text{-cm}^{-1}$ FWHM.

2. Raman spectrum of graphite

In a perfect graphite crystal [single crystal or highly oriented pyrolytic graphite (HOPG)], there is only one Raman-active phonon mode³². It is a zone-center optical mode E_{2g} , corresponding to "in-plane" displacements of atoms strongly coupled in the basal planes and is observed at 1581 cm^{-1} . The Raman spectrum of micro-crystallized graphite³³ consists of two broad bands G and D . Band G (1580 cm^{-1}) is assigned to the only active Raman phonon mode in a perfect graphite crystal. The other band, D (1350 cm^{-1}), becomes Raman allowed because of the symmetry breaking in disordered graphite. Its intensity is inversely proportional to the crystallite size.

3. Raman spectrum of CVD diamond crystals and thin films

Although Raman spectroscopy is known to be a useful characterization technique for detecting a diamond phase in CVD carbon films, few detailed interpretations of this subject have been given.

Matsumoto³ has reported on hot-filament-assisted CVD of diamond films. The Raman diamond line is at 1334 cm^{-1} , with a width of 10 cm^{-1} . Celli,⁸ using the same technique, has obtained similar results: the Raman diamond line is at 1333 cm^{-1} with a width of 12 cm^{-1} . Badzian¹⁵ has carried out Raman microscopy measurements on diamond crystals, deposited with a microwave-plasma-assisted CVD technique. The Raman diamond line of individual crystals is centered at the same position as natural diamond, but its FWHM varies from 5 to 15 cm^{-1} , depending on the nature of the substrate used (graphite or silicon). Broadening of the Raman diamond line is attributed to silicon contamination which acts as a catalyzer. Knight³⁰ has investigated the Raman microspectroscopy of a wide range of diamond films prepared with various CVD techniques. Depending on the substrate hardness, the maximum intensity position of the Raman line shifts in the $1327\text{--}1345\text{ cm}^{-1}$ range. It is attributed to the stresses in the films, either in compression for positive shift or in tension for negative shift.

4. Raman spectra of amorphous DLC films

The Raman spectrum of DLC films, prepared with ion beams or rf sputtering,³⁴ consists of a very broad and asymmetric band (extending more towards low wave number than high wave number). Its maximum intensity is at about 1540 cm^{-1} . With annealing up to 900°C , this band becomes narrower and shifts to the *G* graphite band, while a new band appears in the $1300\text{--}1350\text{ cm}^{-1}$ wave-number range. At 900°C , the Raman spectrum is graphitelike, with the same intensities of the *G* and *D* bands. According to Beeman's model of amorphous carbon,³⁵ the shift of the *G* graphite band to low wave number with amorphization is the result of bond-angle disorder between atoms in sp^2 sites. The movement of the Raman shift of the *D* graphite line towards low wave number, in carbon films prepared with rf sputtering,³⁴ has been attributed to carbon atoms in sp^3 sites.

The electronic and atomic structure of amorphous carbon films has been investigated by Robertson.³⁶ His calculations show that the most stable structure corresponds to compact clusters of carbon atoms in sp^2 sites. The width of the optical gap varies inversely with cluster size. The $\sim 0.5\text{-eV}$ optical gap of *a*-C corresponds to a model of disordered graphite crystals, about 1.5 nm in diameter, bonded by sp^3 sites. The higher optical gap of *a*-CH (1.5–2.5 eV), which is still much smaller than that of diamond (5.5 eV), is the result of hydrogenation which reduces the cluster size rather than saturating the dangling bonds (as in *a*-Si:H).

Ramsteiner³⁷ has studied resonant Raman spectroscopy of *a*-C:H films prepared by rf plasma deposition from hydrocarbon gases. His results are consistent with Robertson's analysis.³⁶ Increasing incident photon energy from 2.18 to 3.54 eV shifts the main Raman band from

1500 to 1600 cm^{-1} . This development is interpreted in terms of scattering from π -bonded carbon clusters, resonantly enhanced for incident photon energies approaching the π - π^* transition energy. Conversely, the Raman band at 1300 cm^{-1} shows almost no variation with photon energy. The difference, between the high- and low-frequency bands, in scattering intensity with photon energy, confirms a heterogeneous two-phase model. Both phases (carbon atoms in sp^2 or sp^3 sites) correspond to different electronic and vibrational structures and the observed Raman spectrum is a combination of their two different phonon spectra. This view is fully consistent with the model of sp^2 -bonded atom clusters connected by sp^3 bonds. Within this model, different cluster sizes can induce a wave-number shift of Raman bands with photon energy. As in polymer chains,³⁸ with the variation of photon wavelength different cluster sizes are probed.

B. Interpretation of the Raman-spectrum modifications with crystal morphology

Our results show similar tendencies to those reported on Raman spectroscopy of CVD diamond. However, the determination of the Raman spectrum of many individual diamond crystals has enabled us to obtain new results on the variation of Raman line shape with crystal morphology.

1. CVD diamond crystals with a (100) front face parallel to the substrate

In Fig. 6(a), the presence of only the diamond Raman signal suggests that no other carbon phases are present in the films. However, the Raman line shape of CVD diamond always differs from that of natural (or synthetic HT,HP) diamond. The Raman structure of well-faceted crystals, with a (100) front face parallel to the substrate, is systematically broader (at least 8.5 cm^{-1}) than that of natural diamond. Furthermore, it is broadened and shifted towards lower wave number.

In order to determine the effect of contamination, x-ray microfluorescence measurements have been undertaken. A few at. % of tungsten was always detected (as a consequence of the nearby hot tungsten filament), but no trace of silicon was found. If the catalytic hypothesis is proposed, it could be induced by tungsten rather than by silicon. However, the broadening and shift to lower energy of the diamond Raman line can be a consequence of other effects.

In a perfect infinite crystal, the photon momentum is extremely small on the scale of the Brillouin zone, and momentum conservation imposes that Raman scattering is only concerned with phonons at the center point Γ of the Brillouin zone. But if disorder takes place on the scale of the phonon mean free path (3–5 nm), the phonon wave function becomes a wave packet localized in real space. Disorder on a distance d induces an uncertainty $\Delta q \sim 1/d$ in the phonon momentum, as large as disorder takes place on a small distance scale. The Raman-active mode is a high-energy one, its energy is maximum at the center point Γ of the Brillouin zone and decreases with q . Thus, a Δq uncertainty in the phonon momentum induces

a broadening of the Raman line shape to low wave number and also shifts the maximum of the phonon density of states to lower energy. In microcrystalline silicon, it has been shown³⁹ that the finite size of spherical crystallites ($\sim 3\text{--}10$ nm) induces a shift towards lower energy and a broadening of the Si Γ'_{25} Raman-active phonon mode. The Raman line becomes asymmetric, more extended, and shifts towards lower wave number. Because of the identical crystal symmetry of silicon and diamond, the same effects should certainly be observed in microcrystalline diamond.

Thus, broadening and shift towards lower wave number of the Raman diamond structure with roughening of the sides of crystals with a (100) front face parallel to the substrate [(a)–(d) in Fig. 6] can be attributed to microcrystallization which is the indication of anisotropic growth of (100) diamond faces.¹⁶ However, the important shift of the Raman diamond structure (c) in Fig. 6 towards lower energy cannot be attributed only to the presence of small grains. It can be the consequence either of ¹³C enrichment with a CVD technique (ascribed to kinetic factors related to differing atomic diffusion of carbon isotopes¹⁵), or of the presence of the hexagonal diamond form as in meteorites.³¹

2. Cubo-octahedric crystals with two (111) and two (100) front faces tilted to the substrate

Crystals which present four tilted faces in front of the substrate [two (100) and two (111)] give a Raman diamond line shifted and broadened to high wave numbers [Fig. 6 and Table I, (f)]. This development of the Raman diamond structure can be the consequence of compressive stresses in the crystallization.³⁰ In view of the way crystals are implanted in the substrate (Fig. 5), it might be hypothesized that accommodation between a flat substrate and cubo-octahedric crystals is more difficult if they grow with (100) and (111) faces tilted to the substrate than if they grow with a (100) face parallel to the substrate.

3. CVD diamond crystals with five twinned (111) faces

Twinning in diamond crystals has often been encountered, and in some cases it gives rise to the growth of five twinned (111) faces. Narayan⁴⁰ has undertaken high-resolution images and microdiffraction studies on pentagonal diamond crystallites grown on Si(100) substrate. Crystallites are oriented in the [011] direction with five (111) twin faces. Presence of twinning, microtwinning, and streaking along the [111] direction and thin slabs of faulted regions have been evidenced. The effect of twinning in the Raman diamond line shape should be rather complicated. From results presented in Fig. 6 and Table I, (e), the fact of obtaining the same position of the Raman diamond line of twinned crystals as of natural diamond, but with a larger FWHM, could be the consequence of both microcrystallization and compressive stresses which induce broadening and shift in opposite directions.

4. Effects of deterioration in crystallization: From well-faceted crystals to blunted crystals and to carbon ball-like elements

Broadening and intensity decrease of the Raman diamond structure, with the appearance of disorder upon growth, is accompanied by the appearance of broad bands (Fig. 7). In comparison with the Raman spectra of graphite, *a*-C and *a*-C:H, those broad bands are attributed to carbon phases other than diamond.

At 1 vol % methane concentration, no trace of graphite is detected (the Raman graphite band *G* at 1575 cm^{-1} is only observed with a 4 vol % methane concentration), but two bands at 1540 and 1350 cm^{-1} appear as the crystallization deteriorates. When the films are composed of faceted crystals, the 1350-cm^{-1} band is the most intense. As crystallization deteriorates, the intensity of the 1540-cm^{-1} band increases more rapidly than that of the 1350-cm^{-1} band. These results are consistent with a two-phase model of *a*-C:H with carbon atoms in sp^2 and sp^3 sites.⁴¹ For a film composed of faceted crystals, the weak intensity of the Raman signal in the $1500\text{--}1600\text{-cm}^{-1}$ range is an indication of very few carbon atoms in sp^2 sites. Consequently, the 1350-cm^{-1} band observed in that film must be induced by amorphous carbon predominantly in sp^3 sites. However, this result seems to be in contradiction with Beeman's calculations,³⁵ which forecast a 1200-cm^{-1} Raman shift in pure sp^3 -bonded amorphous carbon, but no experimental results exist on amorphous diamond. With deterioration of the crystallization, the greater increase of the 1540-cm^{-1} intensity compared to that of 1350 cm^{-1} is the result of the predominance of sp^2 -bonded amorphous carbon growth. The origin of the broad band at 1470 cm^{-1} , which is only visible for films composed of carbon balls [Fig. 7 and Table II (δ)], is more obscure, all the more because it has never been found in *a*-C and *a*-C:H films. It could correspond to sp^2 clusters with much larger disorder in bond angles than those which induce the 1540-cm^{-1} signal.³⁵

V. CONCLUSION

Using a hot-filament-assisted deposition technique it is possible to synthesize diamond crystals and thin films, without any traces of the other carbon phases. However, as with all CVD techniques, results depend crucially on certain experimental parameters. It has not been possible to obtain a homogeneous deposit on an area larger than 1 cm^2 . With a 1 vol % methane concentration in hydrogen, and a 2400-K filament temperature, SEM observations show deposited crystallites of various shapes ranging from cubo-octahedric and well faceted to edgeless and carbon ball-like. Focusing the Raman laser light on individual crystallites has produced evidence of the dependence of the Raman spectrum with crystallization. With deterioration in the diamond crystallization, the Raman spectrum changes from that of pure diamond to that of a mixture of diamond and amorphous carbon.

For the diamond crystals which are the best well facet-

ed, the Raman spectrum shows only the diamond signal. But even there, the Raman diamond line is broader than that of natural diamond. The shape and position of the diamond signal have been shown to depend on crystal growth. Broadening to lower wave numbers (compared with the Raman line of natural diamond) has been attributed to microcrystallization which manifests itself by the roughening of the sides of crystals with a (100) front face parallel to the substrate. For cubo-octahedric crystals, which present four faces tilted to the substrate, shift and broadening of the diamond structure to higher wave numbers have been attributed to stresses in compression. As crystals become edgeless, until they look ball shaped, two broad Raman bands appear at about 1540 and 1355 cm^{-1} . Being consistent with Beeman's calculations³⁵ and Ramsteiner's experimental results,³⁷ the 1540- cm^{-1} band has been attributed to carbon atoms in sp^2 sites, and the 1350- cm^{-1} band to carbon atoms in sp^2 and sp^3 sites, with a predominancy of sp^3 sites with better diamond crystallization.

ACKNOWLEDGMENTS

Support of this research by the Commissariat à l'Energie Atomique, the DMG, and The Laboratoire d'Etudes des Matériaux Minces, and (CEA/DMG/LEMM) is gratefully acknowledged. This work was initiated after many stimulating discussions with Dr. J. Spitz and Dr. S. Paidassi; I would like to express my gratitude to them. The experimental arrangement of the CVD apparatus would not have been operational without the efficient technical assistance of J. P. Chabert and C. Grandjacques. I am indebted to Dr. E. Da Silva for giving access to the Dilor Laser Raman Modular XY spectrophotometer and to the engineers of the Dilor Society for expert technical assistance. I have benefited greatly from very enlightening discussions with Dr. G. Martinez. The Groupe de Physique des Etats Condenses, Département de Physique, Université d'Aix-Marseille II, Faculté des Sciences de Luminy is unité associée au CNRS No. 783.

*Present address: Groupe de Physique des Etats Condensés, Département de Physique, Faculté des Sciences de Luminy, Université d'Aix-Marseille II, Case Postale 901, 13 288 Marseille CEDEX 09, France.

¹B. V. Deryagin and B. V. Spitsyn, Authors' Certificate No. 339131 (1956); B. V. Deryagin, B. V. Spitsyn, A. E. Gorodetzky, A. P. Zakharov, L. L. Builov, and A. E. Aleksenko, *J. Cryst. Growth* **31**, 44 (1975).

²W. G. Eversole, U. S. Patents No. 3 030 187 and No. 3 030 188 (1958).

³S. Matsumoto, Y. Sato, M. Tsutsumi, and N. Setaka, *J. Mater. Sci.* **17**, 3106 (1982).

⁴A. Sawabe and T. Inuzuka, *Appl. Phys. Lett.* **46**, 146 (1985).

⁵H. Kaneko, M. Kamada, R. Kuwae, A. Sawabe, and T. Inuzuka, *Appl. Surf. Sci.* **33/34**, 546 (1988).

⁶Y. Hirose and Y. Terasawa, *Jpn. J. Appl. Phys. Pt. 2* **25**, L519 (1986).

⁷K. Okano, H. Naruki, Y. Akiba, T. Kurosu, M. Iida, and Y. Hirose, *Jpn. J. Appl. Phys. Pt. 2* **27**, L173 (1988).

⁸F. G. Celli, P. E. Pehrsson, H. T. Wang, and J. E. Butler, *Appl. Phys. Lett.* **52**, 2043 (1988).

⁹M. Kamo, Y. Sato, S. Matsumoto, and N. Setaka, *J. Cryst. Growth* **62**, 642 (1983).

¹⁰Y. Sato, M. Kamo, and N. Setaka (unpublished).

¹¹Y. Sato, S. Matsuda, and S. Nogita, *J. Mater. Sci. Lett.* **5**, 565 (1986).

¹²A. R. Badzian, B. Simonton, T. Badzian, R. Messier, K. E. Spear, and R. Roy [*Proc. SPIE* **683**, 127 (1986)].

¹³H. Kawarada, K. S. Mar, and A. Hiraki, *Jpn. J. Appl. Phys. Pt. 2* **26**, L1032 (1987).

¹⁴R. Haubner and B. Lux, *J. Ref. Hard Metals* **6**, 210 (1987).

¹⁵A. R. Badzian, *Mater. Res. Bull.* **23**, 385 (1988); **23**, 531 (1988).

¹⁶K. Kobashi, K. Nishimura, Y. Kawate, and T. Horiuchi, *Phys. Rev. B* **38**, 4067 (1988).

¹⁷K. Kitahama, K. Hirata, H. Nakamatsu, and S. Kawai, *Appl. Phys. Lett.* **49**, 634 (1986).

¹⁸K. Suzuki, A. Sawabe, H. Yasuda, and T. Inuzuka, *Appl. Phys. Lett.* **50**, 728 (1987).

¹⁹T. Miyazawa, S. Misawa, S. Yoshida, and S. Gonda, *J. Appl.*

Phys. **55**, 188 (1984).

²⁰S. Kasi, H. Kang, and J. W. Rabalais, *Phys. Rev. Lett.* **59**, 75 (1987).

²¹E. F. Tchaikovskii, Y. M. Puzikov, and A. V. Semenov, *Kristallografiya* **26**, 219 (1981) [*Sov. Phys.—Crystallogr.* **26**, 122 (1981)].

²²J. Robertson, *Adv. Phys.* **35**, 317 (1986).

²³C. Weissmantel, K. Beligowa, K. Brener, D. Dietrich, U. Ebersbach, M. J. Erler, B. Rau, and G. Reisse, *Thin Solid Films* **96**, 31 (1982).

²⁴H. C. Tsai and D. B. Bogy, *J. Vac. Sci. Technol. A* **5**, 3287 (1987).

²⁵A. M. Bonnot, *Thin Solid Films* (to be published).

²⁶F. Bozso and Ph. Avouris, *Appl. Phys. Lett.* **53**, 1095 (1988).

²⁷S. A. Solin and A. K. Ramdas, *Phys. Rev. B* **1**, 1687 (1970).

²⁸M. Hanfland, K. Syassen, S. Fahy, S. G. Louie, and M. L. Cohen, *Phys. Rev. B* **31**, 6896 (1985).

²⁹R. M. Chrenko, *J. Appl. Phys.* **63**, 5873 (1988).

³⁰D. S. Knight and W. B. White, *J. Mater. Res.* **4**, 385 (1989).

³¹M. Miyamoto, J. Matsuda, and K. Ito, *Geophys. Res. Lett.* **15**, 1445 (1988).

³²R. Al-Jishi and G. Dresselhaus, *Phys. Rev. B* **26**, 4514 (1982).

³³R. J. Nemanich and S. A. Solin, *Phys. Rev. B* **20**, 392 (1979).

³⁴R. O. Dillon, J. A. Woollam, and V. Katkanant, *Phys. Rev. B* **29**, 3482 (1984).

³⁵D. Beeman, J. Silverman, R. Lynds, and M. R. Anderson, *Phys. Rev. B* **30**, 870 (1984).

³⁶J. Robertson and E. P. O'Reilly, *Phys. Rev. B* **35**, 2946 (1987).

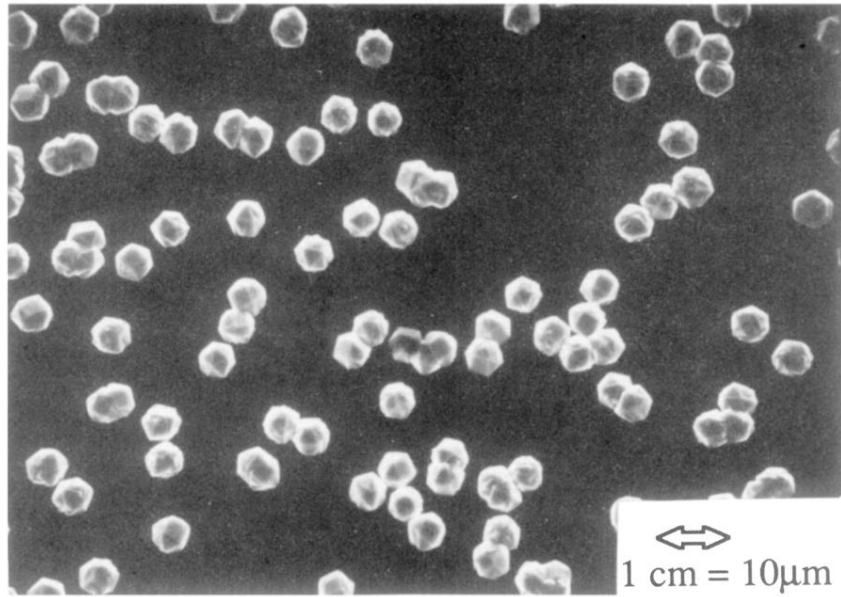
³⁷M. Ramsteiner and J. Wagner, *Appl. Phys. Lett.* **51**, 1355 (1987).

³⁸E. Mulazzi, G. P. Brivio, E. Faulques, and S. Lefrant, *Solid State Commun.* **46**, 851 (1983).

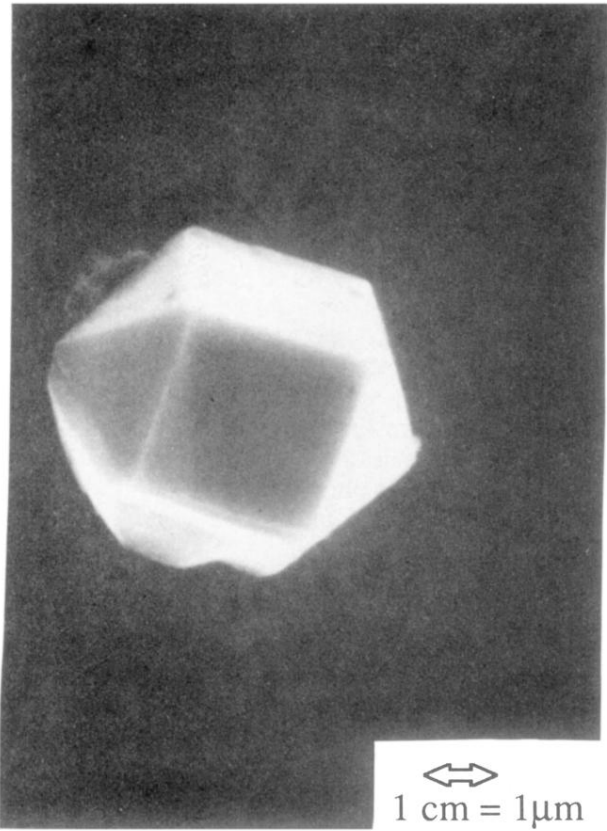
³⁹P. M. Fauchet and I. H. Campbell, *Mater. Sci.* **14**, S79 (1988).

⁴⁰J. Narayan, A. R. Srivatsa, M. Peters, S. Yokota, and K. V. Ravi, *Appl. Phys. Lett.* **53**, 1823 (1989).

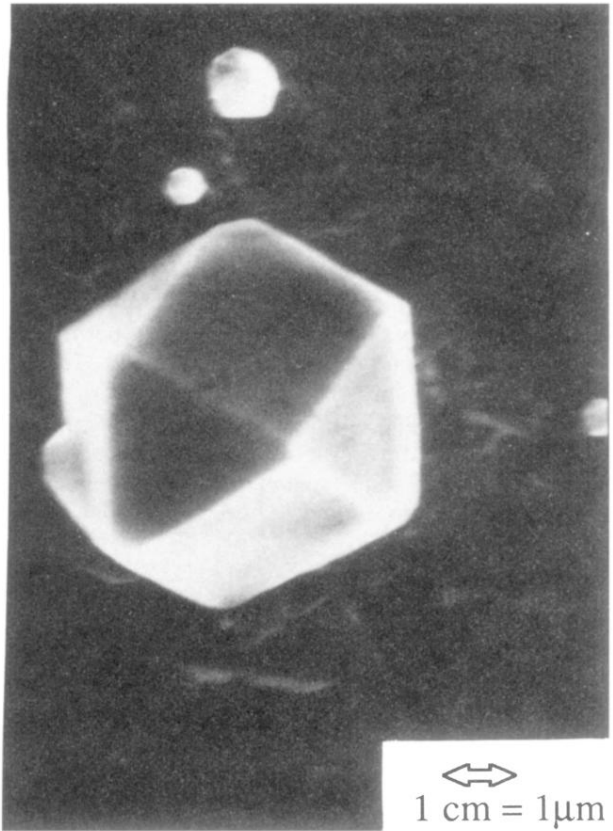
⁴¹H. C. Tsai, D. B. Bogy, M. K. Kundmann, D. K. Veirs, M. R. Hilton, and S. T. Mayer, *J. Vac. Sci. Technol. A* **6**, 2307 (1988).



(a)



(b)



(c)

FIG. 1. SEM micrograph of diamond crystals on silicon.

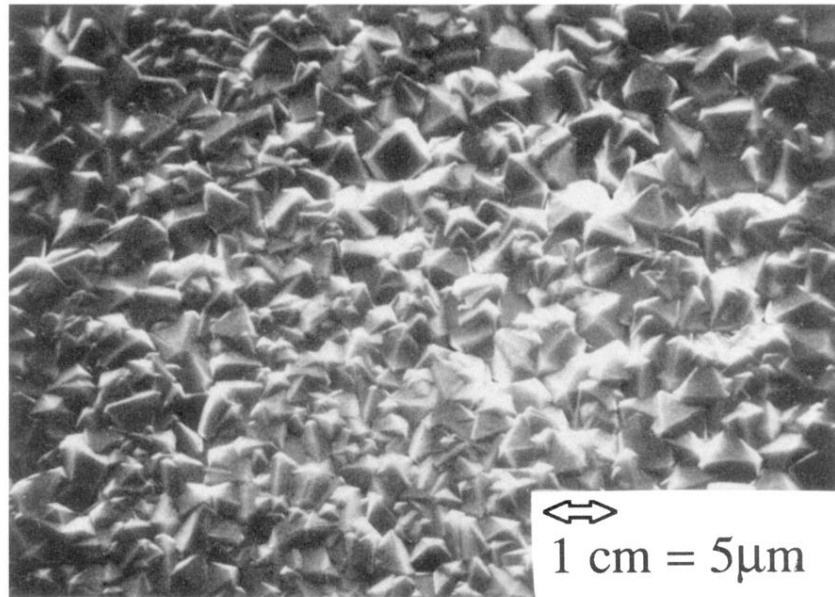


FIG. 2. SEM micrograph of a diamond thin film on a silicon substrate polished with 1- μm diamond paste.

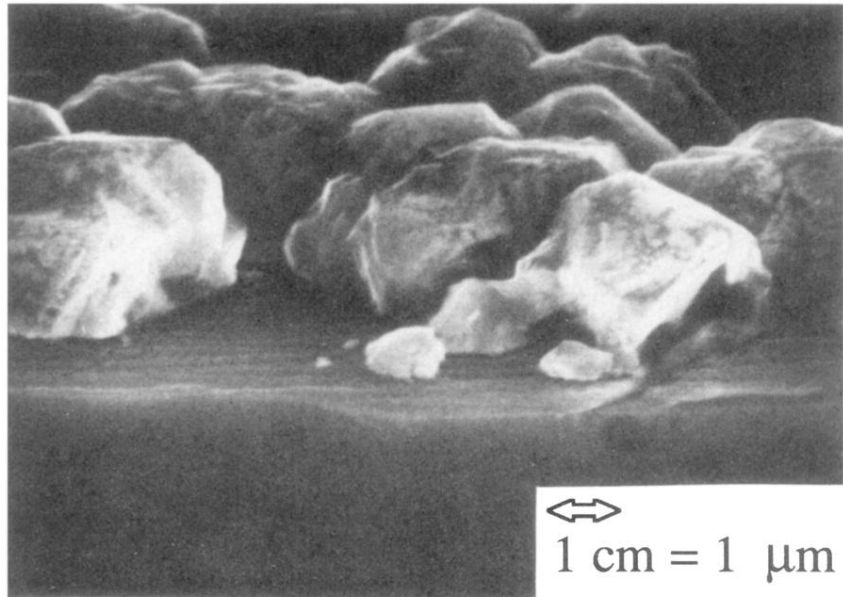


FIG. 3. SEM micrograph of diamond crystals which have lost their edges.

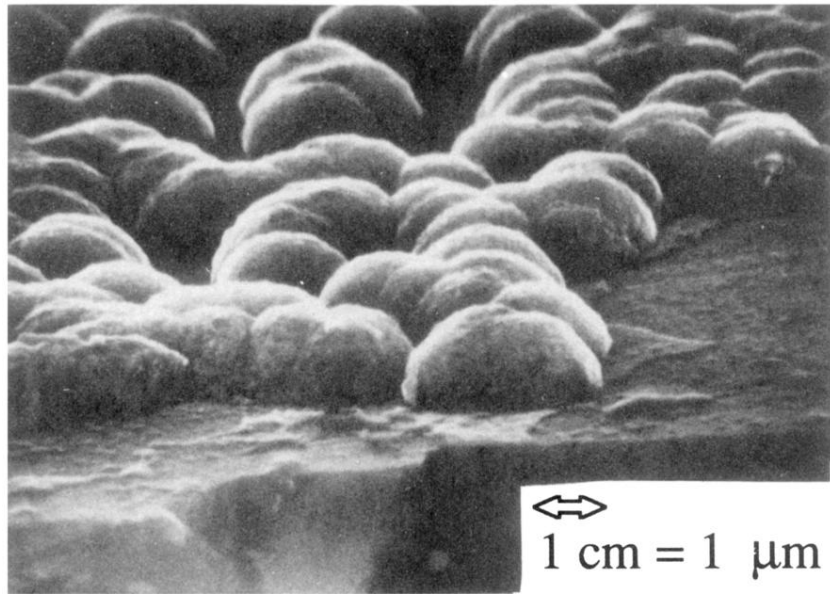


FIG. 4. SEM micrograph of carbon ball-shaped elements.

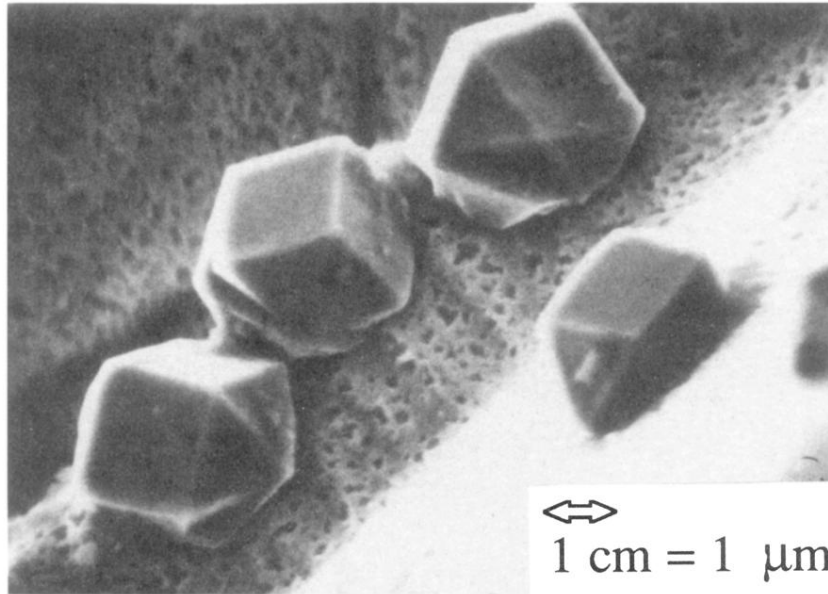


FIG. 5. SEM micrograph showing the way crystals are implanted in the edges of a silicon substrate.